Kinetic Studies of Yeast PolyA Polymerase Indicate an Induced Fit Mechanism for Nucleotide Specificity†

Paul B. Balbo, Gretchen Meinke, and Andrew Bohm*

Tufts University School of Medicine and Department of Biochemistry, Sackler School of Graduate Biomedical Sciences, 136 Harrison Avenue, Boston, Massachusetts 02111

Received January 14, 2005; Revised Manuscript Received March 1, 2005

ABSTRACT: Polyadenylate polymerase (PAP) catalyzes the synthesis of 3′-polyadenylate tails onto mRNA. A comprehensive steady-state kinetic analysis of PAP was conducted which included initial velocity studies of the forward and reverse reactions, inhibition studies, and the use of alternative substrates. The reaction (A_n + ATP ↔ A_{n+1} + PP_i) is adequately described by a rapid equilibrium random mechanism. Several thermodynamic parameters for the reaction were determined or calculated, including the overall equilibrium constant (K_{eq} = 84) and the apparent equilibrium constant of the internal step (K_{int} = 4) which involves the rate-determining interconversion of central complexes. A large (100-fold) difference in V_{max} accounts for nucleotide specificity (ATP vs CTP), despite an only 3-fold difference in K_m. Comparison of the sulfur elemental effect on V_{max} for ATP and CTP suggests that the chemical step is rate-determining for both reactions. Comparison of the sulfur elemental effect on V_{max}/K_m revealed differences in the mechanism by which either nucleotide is incorporated. Consistent with these data, an induced fit mechanism for nucleotide specificity is proposed whereby PAP couples a uniform binding mechanism, which selects for ATP, with a ground-state destabilization mechanism, which serves to accelerate the velocity for the correct substrate.

Polyadenylate polymerase (PAP)[1] of yeast is a template-independent RNA polymerase (*1*−*4*) that functions in the nucleus and is responsible for the polyadenylation of messenger RNA (reviewed in refs *5* and *6*). Yeast PAP is a catalytic subunit of the cleavage/polyadenylation factor (CPF), a large protein complex responsible for RNA 3′-end processing (*7*−*11*). Many of the functions of RNA 3′-end processing are mediated by other CPF subunits. These functions include recognition of cis elements which define the correct polyadenylation site on the pre-mRNA, catalysis of specific endonucleolytic cleavage at the polyA site, regulation of polyA tail length (50−90 bases in yeast; 250 in mammals), and the termination of polyadenylation (*7*, *12*−*21*). Polyadenylation of transcripts in vivo is thought to be processive, where processivity is defined as the ability of the enzyme to undergo multiple cycles of adenylyl transfer without intermittent RNA dissociation. Processive polyadenylation requires a number of other proteins which appear to act primarily by binding the RNA, thus tethering it to the polymerase via protein−protein interaction occurring within the CPF complex (*22*). In vitro, PAP can polyadenylate any RNA or single-stranded DNA but shows a preference for polyriboadenylate (*3*, *23*). Recently, several reports concerning the identification of 3′-end processing factors and their physiological roles in the regulation of polyadenylate synthesis have appeared (*24*−*32*). To understand how polyadenylation is affected by interactions with other CPF subunits, it is essential to characterize the biochemical properties intrinsic to the polymerase itself.

Despite the X-ray structures of the yeast (*33*) and bovine (*34*, *35*) polyA polymerase enzymes and a number of mutational studies (*35*−*39*), many fundamental biochemical properties of PAP, including the determinants important for binding of the RNA substrate and the mechanism of nucleotide specificity, are still poorly understood. A representation of the X-ray structure of yeast PAP is shown in Figure 1. PAP is organized into three globular domains (Figure 1A), the orientation of which defines a broad active site cleft (approximately 35 Å long, 25 Å high, and 12 Å wide). The N-terminal domain is structurally similar to the "palm" domain of other enzymes in the DNA polymerase β family which includes CCA adding enzymes, terminal deoxynucleotidyl transferases, 2′−5′ synthetases, and antibiotic nucleotidyl transferases (*40*). Located in this domain are three conserved Asp residues (D100, D102, and D154), which are required for catalysis and participate in the coordination of two Mg^{2+} ions. One metal (Figure 1B) binds as a cosubstrate (as $MgATP^{2-}$) and leaves with the product in the form of $MgPP_i^{2-}$. The other metal functions catalytically to stabilize the negative charge that develops at the transition state and to orient the reacting groups of the substrates (*41*−*44*). In the yeast PAP structure, two nucleotides and two metals are bound at the active site (*33*). The positions of these two nucleotides define two subsites within the active site: (1) the ATP subsite, which is occupied by the incoming nucleotide triphosphate, and (2) the polyA

† Supported by NIH Grant RO1 GM065972.

* To whom correspondence should be addressed. Phone: (617) 636-2994. Fax: (617) 636-2409. E-mail: andrew.bohm@tufts.edu.

[1] Abbreviations: PAP, polyadenylate polymerase; A_n, polyadenylate (*n* is the number of residues); PP_i, pyrophosphate; AMP-CPP, α,*β-methylene*-ATP; αS-ATP, [α-thio]ATP.

10.1021/bi050089r CCC: $30.25
Published on Web 05/06/2005

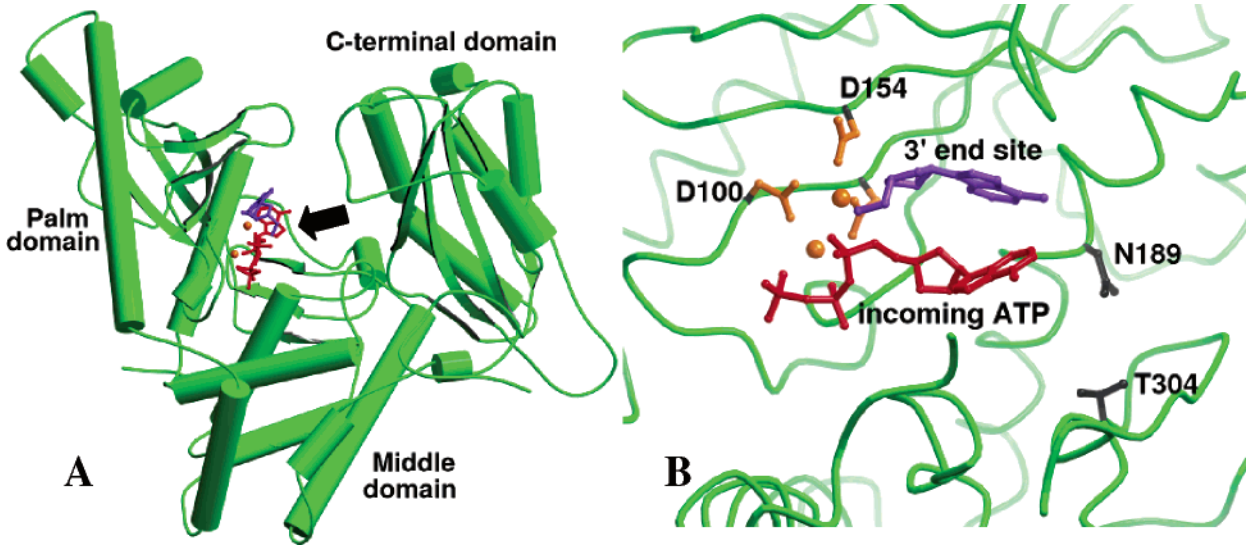

FIGURE 1: PolyA polymerase structure. The domain organization of PAP is shown in panel A. At the active site, located at the base of the broad cleft, are the incoming nucleotide (red), the nucleotide representing the 3′-terminus of the polynucleotide substrate (violet), and the two metal ions (orange). A detailed representation of the active site is shown in panel B. The orientation of the view in panel B is denoted by the arrow in panel A and looks toward the surface of the active site from within the cleft. The locations of the ATP subsite and polyA subsite, as described in the text, are indicated in panel B by the positions of the incoming nucleotide (red) and the 3′-end site (violet), respectively. Also labeled are two of the three catalytic Asp residues, D100 and D154 (the third, D102, is obscured behind the nucleotide at the 3′-end site). Two conserved residues, N189 and T304, implicated in the recognition of the adenine base of ATP (*35*) are colored gray. Movement of the N-terminal (palm) domain toward the middle domain would enable contact between these residues and the bound ATP substrate.

subsite, which is presumably occupied by the 3′-end of the polyA substrate during catalysis. The stereochemistry of these nucleotides and the two metal ions is similar to that seen in the other polymerase structures (*35*, *42*, *43*, *45*−*49*). The yeast structure shows three specific contacts involving the adenine ribose portion of the nucleotide bound at the polyA subsite. These include a stacking interaction between V141 and the adenine base and a hydrogen bond between N6 of the base and the main chain carbonyl of R186 (*33*). No structure to date has revealed significant binding determinants for polyA other than those to the 3′-terminus, nor has any structure of a PAP−RNA complex yet been reported.

The structural basis for nucleotide specificity is poorly understood. The yeast structure reveals no adenine-specific contacts involving the nucleotide bound at the ATP subsite (*33*). However, the angle between the N-terminal and middle domains differs by 5° between the two molecules in the yeast asymmetric unit, suggesting that further domain movements could bring the adenine of ATP into the proximity of residues located in the middle or C-terminal domains (Figure 1A). Alternatively, base-specific contacts between the enzyme and ATP may be achieved through the rotation of the adenine group of the nucleotide at the ATP subsite. Martin et al. (*35*) recently determined the structure of bovine PAP in the presence of Mg^{2+} and 3′-deoxy-ATP. In this structure, the interdomain angle is 2.5° smaller than that seen in the earlier bovine structure, consistent with the idea of conformational flexibility. The authors identified a number of specific protein contacts involving the adenine moiety of this nucleotide, including an interaction between the N1 atom and a conserved Gln and Thr (N189 and T304 in yeast) as well as a number of hydrophobic residues observed in the proximity of the adenine ribose. Site-directed mutagenesis studies were performed, but the majority of these had no significant effect on the apparent K_m for ATP (a notable exception was T304, which had a 4-fold effect on both K_m and V_{max}). Interestingly, mutation of many of the residues located in the ATP subsite had an effect on the apparent K_m for RNA. Taken together, the current body of biochemical and structural information does not satisfactorily explain nucleotide specificity. Certainly, the effort to identify residues that are important in ATP binding and specificity has so far been hindered by both an inability to obtain crystals of an enzyme−ATP−RNA ternary complex and the lack of detailed knowledge of the kinetic mechanism.

To gain insight into the determinants for substrate binding and nucleotide specificity, a thorough steady-state kinetic analysis was conducted for the reaction $A_n + ATP \leftrightarrow A_{n+1} + PP_i$. Both the forward (polyadenylation) and reverse (pyrophosphorolysis) directions were studied. This included inhibition studies and the use of alternative substrates. The data are consistent with a rapid equilibrium random mechanism for both of the reactions using either ATP or the alternative substrate, CTP. From these data, various internal thermodynamic parameters for the enzyme under the steady state have been calculated. This analysis indicates that both the internal thermodynamics and competition between ATP and A_n (product mode) binding effectively control the direction of the reaction such that polyadenylation is strongly favored over pyrophosphorolysis. Comparison of the kinetic parameters for ATP and CTP indicates that nucleotide specificity is largely manifested in the maximal rates of reaction. To gain additional insight into the nature of the rate-determining step, the sulfur elemental effect of [α-thio] substitution on both ATP and CTP was studied. Under conditions of nucleotide saturation (i.e., V_{max} conditions), both substrates exhibited similar elemental effects, consistent with both reactions being rate-limited by an identical step. In contrast, inspection of the kinetic parameters under subsaturating conditions (i.e., V_{max}/K_m conditions) revealed differences between the mechanisms for the two nucleotides. The results indicate that ATP utilizes a ground-state destabiliza-

tion mechanism for rate acceleration, whereas CTP does not. From the alternative substrate kinetic and elemental effect data, the following induced fit mechanism is proposed. Nucleotide specificity is mediated by stabilization of both the transition state and ground state (uniform binding) using free energy derived from the recognition of the adenine moiety of ATP, and rate acceleration is effected by the utilization of this binding energy in increasing the free energy of the ground state (ground-state destabilization). Finally, the relevance of the data to kinetic models of polymerase mechanisms and to processive polyadenylation in vivo is discussed.

MATERIALS AND METHODS

Chemicals. All chemicals and buffers were of analytical quality. The following chemicals were purchased from Sigma-Aldrich: ATP, α,*β-methylene*-ATP (AMP-CPP), and pyrophosphate (PP_i). The α-thio derivatives of ATP and CTP were purchased from TriLink (San Diego, CA). Disodium dATP, CTP, and [^{35}S][α-thio]ATP and -CTP were purchased from MP Biomedicals (Irvine, CA). Luciferin and luciferase were purchased from Promega (Madison, WI). Oligo RNAs (2′-deprotected, and either PAGE- or HPLC-purified) were purchased from Dharmacon (Lafayette, CO). Nucleotide concentrations were determined by UV absorbance using their published molar absorptivity values. RNA concentrations were determined using their theoretical molar absorptivity values. [2,8-^{3}H]ATP and [5-^{3}H]CTP were purchased from PerkinElmer (Boston, MA) as 50% ethanol solutions. Prior to their use, the ethanol was removed by applying a steady stream of air over the surface of the solution, and the amount of radionucleotide was redetermined by liquid scintillation counting using the specific activity provided by the supplier.

PolyA Polymerase. All experiments utilized a recombinant yeast PAP that had a 32-amino acid C-terminal truncation and included a C-terminal His_6 tag to facilitate purification (henceforth in this paper termed PAP). The construct was generated by PCR using full-length PAP as the DNA template, the upstream primer CATATGAGCTCTCAAAAGGTTTTTGGT, and the downstream primer CTCGAGATTCTTCCTTTTACTCTTCTTTGA. PCR products were purified and cloned into a Pet21b plasmid using NdeI and XhoI restriction sites. The encoded protein includes residues 1−537 of *Saccharomyces cerevisiae* PAP followed by a LEHHHHHH sequence. PAP concentrations were determined by the absorbance at 280 nm ($\epsilon_{280}^{0.1\%} = 0.99$ L g^{-1} cm^{-1}). Small, single-use aliquots were frozen in N_2(l) for storage and thawed prior to use. The 32-amino acid truncation of PAP (without the His tag) has been previously shown to exhibit wild-type activity (*36*), and the activity is unaffected by the addition of the His_6 tag (data not shown). PAP was purified by nickel affinity and anion exchange chromatography using NTA agarose (Qiagen) and Source S (Pharmacia) resins. The final yield of pure protein is ∼5 mg/L of *Escherichia coli* culture.

Polyadenylation Kinetics. The initial rates of polyadenylation were determined at 30 °C using a discontinuous assay assessing the incorporation of [^{3}H]AMP into substrate oligo RNAs, similar to those previously described (*23*). Briefly, the reaction components were mixed (without enzyme) in a total volume of 20 μL and allowed to thermally equilibrate for 15 min. Unless otherwise stated, the reaction buffer conditions were as follows: 40 mM bis-Tris (pH 7.0), 20 mM NaCl, 1 mg/mL BSA, 10% glycerol, 10 mM *β*-mercaptoethanol, 1 mM spermine, 0.01% Nonidet-P 40, and 10 mM $MgCl_2$. We observed a decay of PAP activity with a half-life of approximately 2 h (on ice) if NP-40 was omitted from the enzyme storage solution. During preliminary studies, the Mg^{2+} concentration that resulted in half-maximal activity was determined to be 1.5 mM, and no apparent inhibition was observed as high as 15 mM Mg^{2+}. Substrate concentrations varied depending on the experiment; the ranges of these were from 2 to 200 μM for RNA and from 5 to 500 μM for ATP. The reaction was initiated by the addition of an appropriate amount of PAP (6 nM PAP for ATP + A_{18} reactions, 60 nM PAP for ATP + A_{17}C reactions, and 200 nM PAP for CTP + A_{18} reactions). Aliquots (2 μL) of the reaction were removed and quenched by the addition of 150 μL of ice-cold 15% TCA at 1 min intervals during the first 4 min of the reaction. It was calculated from the velocity data that during this period, 0.5−6% of the oligonucleotide substrates were modified by nucleotidylation, on average. The quenched reaction mixtures were incubated on ice for 30 min and then centrifuged at 16 000 rpm for 20 min at 4 °C. The precipitated pellet containing the elongated RNA was washed with ice-cold 15% TCA and then redissolved in 10 mM NaOH and 0.1% SDS. The amount of tritium in the samples was then measured by liquid scintillation counting. Analogous procedures were used to measure the PAP-catalyzed rates of [^{3}H]CMP incorporation from [^{3}H]-CTP and [^{35}S]AMP or -CTP incorporation from [^{35}S]-αS-ATP or -CTP, respectively.

Pyrophosphorylation Kinetics. The initial rates of pyrophosphorylation of A_{18} were determined at 30 °C by measuring the concentration of ATP formed during the reaction by the discontinuous luciferin/luciferase assay (*50*). Buffer conditions were generally the same as those for polyadenylation reactions (see the text for specific details). All reaction components (except enzyme) were combined and thermally equilibrated prior to the initiation of the reaction by the addition of an appropriate amount of PAP. Reactions (2 μL) were stopped periodically by the addition of 100 μL of 1 mM EDTA. Samples were then frozen until they were subjected to analysis by the luciferin/luciferase assay. The luciferase assay buffer (prepared fresh prior to use) contained 30 mM Tris (pH 7.8), 6 mM $MgCl_2$, 5 mM *β*-mercaptoethanol, 1 mg/mL BSA, 10 μM luciferin, and 150 nM luciferase. Assays were performed by mixing 10 μL of the EDTA-stopped sample with 80 μL of buffer and then measuring the light produced with an Optocomp-P luminometer (MGM Instruments). ATP concentrations in the samples were determined by comparison to a reference ATP curve (ATP was standardized by A_{260}).

Calculation of $MgATP^{2-}$ and $MgPP_i^{2-}$ Concentrations. At physiological pH and Mg^{2+} concentrations, ATP and PP_i are present in solution as magnesium complexes. Therefore, the concentrations of these reactants are presented throughout this work as those of their monomagnesium complexes. The concentrations of $MgATP^{2-}$ and $MgPP_i^{2-}$ as a function of the free Mg^{2+} concentration were calculated from the dissociation constants (describing $Mg_2L^0 \leftrightarrow MgL^{2-} + Mg^{2+}$)

of Mg_2ATP and Mg_2PP_i, which are 16.7 and 4.6 mM, respectively (*51*).

Data Analysis. The initial rate data were fitted by nonlinear regression to the appropriate rate equation by applying a relative weight ($1/Y^2$) to the data, using the program gnuplot. In cases where a single data set was fit to different models, the goodness of fit was compared by the relative χ^2 parameter [χ^2/(*n* degrees of freedom)], but in most cases, the choice of model could be determined by visual inspection of the double-reciprocal plot of the data. Initial velocity data were analyzed according to the bireactant sequential reaction model given in eq 1. Dead-end and product inhibition data sets were analyzed according to the following equations for competitive (eq 2), and noncompetitive inhibition (eq 3) as appropriate, where *A* is the variable substrate and *V* and *K* are substrate-dependent constants. When substrate inhibition was considered, the term A^2/K_I was added to the denominator of the appropriate rate equation. Throughout the paper, reactant concentrations are represented as follows: $A = [A_n]$ (or alternative RNA substrate), $B = [MgATP^{2-}]$ (or $[MgNTP^{2-}]$), $P = [MgPP_i^{2-}]$, and $I =$ [inhibitor]. The Michaelis constants (K_a, K_a', and K_{ia} for A_n, K_b and K_{ib} for ATP, and K_p and K_{ip} for PP_i) conform to the notation of Cleland (*52*) and are further described in the text. When pyrophosphorolysis was studied, eq 1 was modified by substituting *B* with *P*, K_a with K_a', and K_b with K_p.

$$v = \frac{VAB}{K_{ia}K_b + K_aB + K_bA + AB} \quad (1)$$

$$v = \frac{VA}{K(1 + I/K_{is}) + A} \quad (2)$$

$$v = \frac{VA}{K(1 + I/K_{is}) + A(1 + I/K_{ii})} \quad (3)$$

RESULTS

Steady-State Kinetics of Polyadenylation. A characteristic feature of polymerase reactions is that one of the reactants (the polymer) serves as both a substrate and product (*53*−*55*). Consequently, the definitions of certain kinetic parameters differ from the ordinary case of a bireactant system, even though the general form of the steady-state bireactant mechanism, eq 1, applies (see the Discussion). In the forward direction, the initial velocity as a function of $[MgATP^{2-}]$ and $[A_{18}]$ was measured at 10 mM Mg^{2+}, and the data were fit to eq 1. The results are shown in Figure 2, and the kinetic parameters are reported in Table 1. Additionally, the kinetics of two pairs of alternative substrates was studied by analogous experiments: (1) cytidylate transfer onto A_{18} (utilization of $MgCTP^{2-}$) and (2) adenylate transfer onto $A_{17}C$. These results (data not shown) are also reported in Table 1. The kinetic parameters reported for these alternative substrates describe the reaction for a single nucleotidyl transfer event. Note that although the K_m values for ATP and CTP (K_b) differed by a factor of only 3, a substantial velocity effect (~300-fold difference in V/K_m) was observed. To confirm the K_m result for CTP, a separate experiment was performed where CTP was employed as a competitive inhibitor of ATP in the reaction of [^{3}H]ATP with A_{18} (data not shown). The Michaelis inhibition constant derived from this experiment corresponds to the K_b for CTP and was 63.7 ± 14.0 μM, in agreement with the data reported in Table 1. The reactions of ATP and CTP with A_{18} also provide an independent measure of K_{ia}, which agree within error. Interestingly, modification of the 3′-terminal residue from A to C ($A_{17}C$ reaction) lowered the maximum velocity by 10-fold and affected the K_m for ATP. This result suggests that binding and recognition of the polynucleotide substrate are important for efficient adenylyl transfer, possibly by promoting the proper conformational organization of the active site for catalysis.

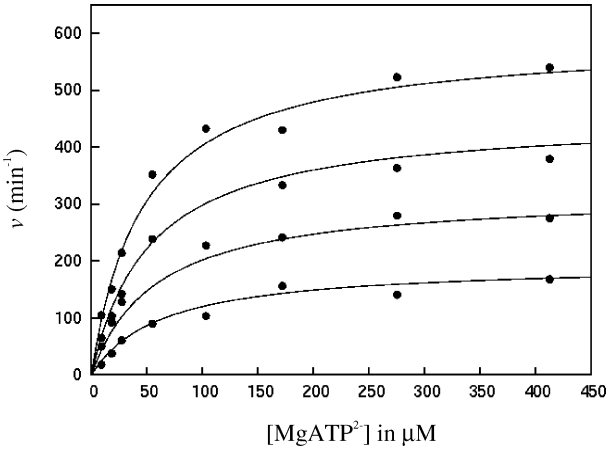

FIGURE 2: Initial velocity of polyadenylation by PAP. The initial velocity of polyadenylation at 10 mM Mg^{2+} as a function of $MgATP^{2-}$ concentration at various, fixed A_{18} concentrations is shown. The data sets (from bottom to top) correspond to 14.1, 28.3, 54.2, and 108.3 μM A_{18}. The curves were generated using the experimentally derived parameters (reported in Table 1).

Table 1: Steady-State Kinetic Parameters for PolyA Polymerase

Forward (Polyadenylation) Direction			
	A_{18} and $MgATP^{2-}$	A_{18} and $MgCTP^{2-}$	$A_{17}C$ and $MgATP^{2-}$
V_1 (min^{-1})	845.8 ± 126.5	8.6 ± 1.9	86.3 ± 16.7
K_a (μM)	46.8 ± 12.4	64.2 ± 22.5	26.3 ± 8.9
K_{ia} (μM)	93.2 ± 28.9	71.0 ± 18.1	21.2 ± 7.9
K_b (μM)	35.9 ± 12.6	103.6 ± 36.2	123.0 ± 43.5
K_{ib} (μM)	71.5 ± 22.2	114.6 ± 29.2	99.1 ± 36.9

Reverse (Pyrophosphorylation) Direction	
	A_{18} and $MgPP_i^{2-}$
V_2 (min^{-1})	189 ± 296
K_a' (mM)	2.27 ± 3.60
K_p (μM)	671 ± 1100
K_{ip} (μM)	28 ± 46

Inhibition Studies. Initial velocity experiments alone are insufficient to differentiate between ordered and random reaction mechanisms. Therefore, as part of the effort to determine the steady-state mechanism (for the reaction of ATP and A_{18}), inhibition experiments were performed using either the dead-end inhibitor, AMP-CPP (a nonreactive ATP analogue), or the product inhibitor, pyrophosphate. In the case of random substrate binding, the predicted inhibition patterns for polymerase-type reactions are identical to the ordinary bireactant system except that PP_i is expected to be noncompetitive versus A_{18} rather than competitive (*54*). Chao et al. (*53*) noted that the inhibition patterns for the ordered polymerase mechanisms differ more substantially from those of the ordinary bireactant case. In these experiments, the initial velocity was measured as a function of the variable

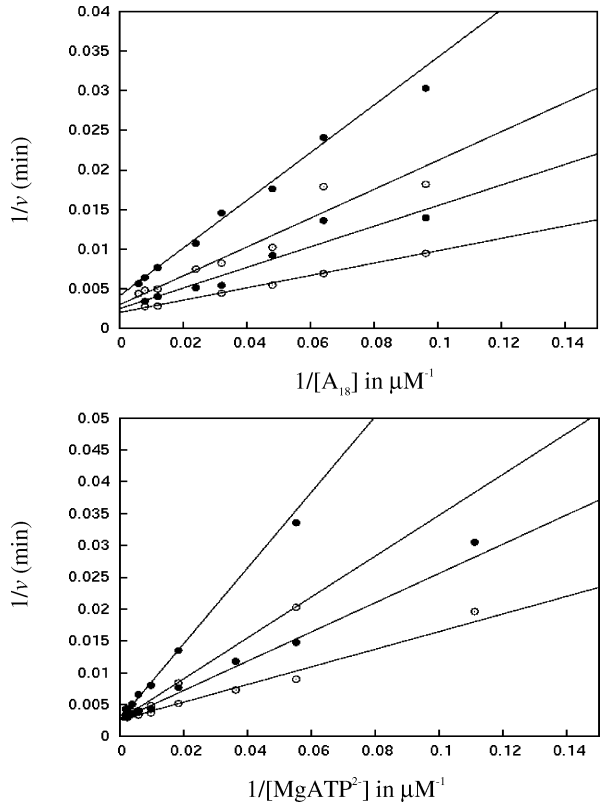

FIGURE 3: Dead-end inhibition of PAP by AMP-CPP. The initial velocity was measured as a function of either A_{18} (top) or $MgATP^{2-}$ (bottom) concentration at various, fixed concentrations of the inhibitor at 10 mM Mg^{2+}. AMP-CPP is a nonhydrolyzable ATP analogue. The concentrations (top) of AMP-CPP were 0, 51.6, 103.2, and 221.2 μM; $[MgATP^{2-}] = 35.6$ μM. The concentrations (bottom) of AMP-CPP were 0, 49.0, 98.0, and 245.0 μM; $[A_{18}] = 64.3$ μM. The data were analyzed by nonlinear regression (gnuplot), and the derived parameters were used to prepare the Lineweaver–Burk plots.

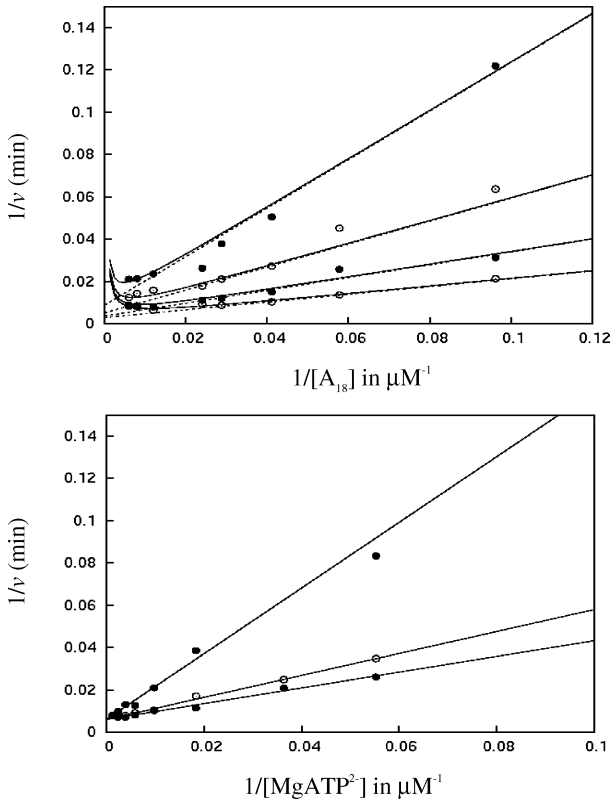

FIGURE 4: Product inhibition of PAP by PP_i. The initial velocity was measured as a function of either A_{18} (top) or $MgATP^{2-}$ (bottom) concentration at various, fixed concentrations of the inhibitor at 2 mM Mg^{2+}. The concentrations (top) of $MgPP_i^{2-}$ were 0, 22.5, 67.5, and 181.0 μM; $[MgATP^{2-}] = 80.0$ μM. The concentrations (bottom) of $MgPP_i^{2-}$ were 0, 22.6, and 181 μM; $[A_{18}] = 49.8$ μM. In the top panel, the solid lines correspond to the solution for the noncompetitive model with substrate inhibition (SI); dashed lines correspond to the same solution except with no SI.

substrate concentration at various, fixed concentrations of inhibitor. The results for inhibition by AMP-CPP, presented in the Lineweaver–Burk format, are shown in Figure 3. AMP-CPP was competitive versus ATP ($K_{is} = 74.3 \pm 6.3$ μM) and noncompetitive versus A_{18} ($K_{is} = 77.4 \pm 12.6$ μM, $K_{ii} = 210.7 \pm 64.1$ μM). The inhibition constant K_{is} describes the $E{\cdot}I \leftrightarrow E + I$ equilibrium, and K_{ii} describes the $E{\cdot}A_n{\cdot}I \leftrightarrow E{\cdot}A_n + I$ equilibrium (*54*). This result provides strong evidence against an ordered binding mechanism for which uncompetitive inhibition versus A_{18} is predicted.

Distinction between rapid equilibrium and steady-state random mechanisms can sometimes be made on the basis of product inhibition (*52*). For the polymerase-type mechanism, noncompetitive inhibition versus both ATP and A_{18} is consistent with a steady-state random mechanism, whereas competitive inhibition versus ATP and noncompetitive inhibition versus A_{18} are consistent with a rapid equilibrium mechanism (*54*). The product inhibition data, presented in the Lineweaver–Burk format, are shown in Figure 4. In these experiments, the Mg^{2+} concentration was lowered to 2 mM to prevent precipitation that occurs with high PP_i concentrations at 10 mM Mg^{2+}. Apparent substrate inhibition by A_{18} was observed at 2 mM (Figure 4) but not at 10 mM Mg^{2+}. It is likely that this inhibition is the result of the loss of enzyme activity because of the lower ion activity of Mg^{2+} at higher A_{18} concentrations (data not shown); this phenomenon has been described previously (*56*, *57*). However, using the substrate inhibition correction does allow for the accurate determination of the steady-state kinetic parameters for pyrophosphate. Pyrophosphate was competitive versus ATP ($K_{ip} = 34.0 \pm 2.9$ μM) and noncompetitive versus A_{18} ($K_p = 28.7 \pm 8.4$ μM, $K_{ip} = 16.2 \pm 2.1$ μM), where K_p and K_{ip} refer to inhibition constants affecting the intercept and slope terms, respectively. These results are consistent with a rapid equilibrium random mechanism. According to Gold et al. (*54*), the dissociation constant K_{ip} describes the $E{\cdot}PP_i \leftrightarrow E + PP_i$ equilibrium and K_p describes the $E{\cdot}A_n{\cdot}PP_i \leftrightarrow E{\cdot}A_n + PP_i$ equilibrium. Pyrophosphate can bind to either of two enzyme–A_n complexes to form either an $E'{\cdot}A_n{\cdot}PP_i$ ternary product complex or an $E{\cdot}A_n{\cdot}PP_i$ dead-end complex (with A_n bound in a substrate-binding mode). The results described further below suggest that the formation of the dead-end complex is significantly more favorable than formation of the ternary product complex. Thus, we conclude that the value of "K_p" derived from this experiment is not equal to the Michaelis constant for PP_i in the reverse direction, but is a second inhibition constant as defined above.

A criticism of the product inhibition experiment is that small velocity effects can be difficult to detect, thus making truly noncompetitive inhibition patterns appear to be competitive. With regard to this concern, it is noted that the initial velocity experiment utilizing the alternative substrate, CTP, yields an independent measurement of K_{ia} and thus provides

Scheme 1: Rapid Equilibrium Random Mechanism for Polyadenylate Polymerase

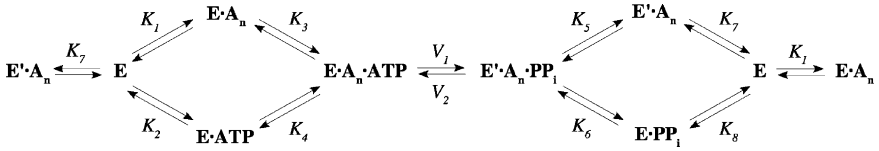

corroborative evidence that the rapid equilibrium assumption is valid. For a rapid equilibrium mechanism, K_{ia} reflects only the apparent binding constant (see the Discussion) of A_{18} for the free enzyme (*53*). In a steady-state mechanism (i.e., one in which the rate of substrate dissociation is slower than or on the order of the rate of conversion of central complexes), K_{ia} is a more complex function of the various rate constants, including k_{cat} (*58*, *59*), and thus should be different in the ATP and CTP reactions. The agreement between these values suggests that substrate dissociation is fast relative to the internal conversion step, consistent with the rapid equilibrium model. In summary, the data described above together are consistent with a rapid equilibrium random substrate binding mechanism.

Steady-State Kinetics of Pyrophosphorolysis. The kinetics of pyrophosphorolysis was also studied. The initial velocity for the reverse reaction as a function of [$MgPP_i^{2-}$] and [A_{18}] was measured at 10 mM Mg^{2+}, and the data were fit to eq 1. The results are shown in Figure 3, and the kinetic parameters are reported in Table 1. In this analysis, K_{ia} was treated as a fixed parameter and set equal to the value determined in the polyadenylation experiment (in the polymerase mechanism, K_{ia} represents the composite binding constant of A_{18} for the free enzyme, and is identical in both the forward and reverse directions). The standard errors for the fit parameters were high because of the experimental inaccessibility of the high A_{18} and $MgPP_i^{2-}$ concentrations needed to properly sample the velocity curves. Given this difficulty, the data fit better to the sequential random model (χ^2/ndf = 1.7) than to the rapid equilibrium ordered model (χ^2/ndf = 4.2). Despite the high standard errors, the K_{ip} value (28 μM) reported in Table 1 is in close agreement with the K_{ip} values derived from the product inhibition experiments.

Sulfur Elemental Effect on the Reactions Using ATP and CTP. The elemental sulfur effect on the forward reaction was studied using the α-thio derivatives of both ATP and CTP. The sulfur elemental effect is derived from the different electron withdrawing effects of the substituted sulfur, relative to the oxygen atom, at the nonbridging position. The phosphorothioate exhibits a lower intrinsic chemical reactivity because of the weaker stabilization of the negative charge that develops at the transition state (*60*−*62*). This type of experiment can provide insight about the enzyme mechanism, including the importance of the chemical step relative to substrate binding or conformational change steps on rate limitation. When chemistry is completely rate limiting, model studies suggest that an elemental effect of 4−10 is expected for this reaction; the absence of an elemental effect is consistent with a rate-limiting binding or conformational change step (*62*). Here, pseudo-first-order reactions, at a constant [A_{18}], were studied, and the velocity dependence on either [NTP] or [αS-NTP] was measured. The parameters V and V/K_m were compared, where V and K_m are apparent constants. For ATP, $(V/K_m)_{phosphate}/(V/K_m)_{phosphorothioate} = 1.2 \pm 0.4$ and $(V)_{phosphate}/(V)_{phosphorothioate} = 3.6 \pm 0.3$. For CTP, $(V/K_m)_{phosphate}/(V/K_m)_{phosphorothioate} = 3.0 \pm 1.2$ and $(V)_{phosphate}/(V)_{phosphorothioate} = 3.2 \pm 0.5$. The similar elemental effect on V for both ATP and CTP suggests that both reactions are rate-limited by an identical step. Furthermore, the absolute value of this effect is consistent with a rate-determining chemical step under conditions of nucleotide saturation; albeit, this conclusion is somewhat tenuous (*62*). Both of these conclusions are consistent with the steady-state kinetic data. The sulfur elemental effect on V/K_m (the second-order rate constant for the reaction of E·A_n with nucleotide) differs for the two alternative substrates, ATP and CTP. For ATP, both V and K_m are affected by essentially the same degree; thus the sulfur elemental effect on V/K_m is unity. This suggests a ground-state destabilization mechanism for ATP (*63*, *64*). It will be discussed below that this difference reflects the different utilization of binding energy by the enzyme to promote catalysis for the correct and incorrect nucleotide substrates.

DISCUSSION

This report addresses several aspects of the enzymology of polyadenylation in yeast. The steady-state kinetics in both the forward (polyadenylation) and reverse (pyrophosphorolysis) directions were studied. Furthermore, the comparison of the steady-state kinetic parameters of the enzyme utilizing ATP and alternative nucleotide substrates has provided insight into the mechanism for substrate specificity. The results establish that the steady-state mechanism of PAP, illustrated in Scheme 1, is rapid equilibrium random. According to Scheme 1, the polyA substrate (A_n) can bind in either of two mutually exclusive binding modes. It is reasonably assumed that A_n and the product, A_{n+1}, are chemically indistinguishable at the active site (both having 3′-terminal adenylate residues); thus, both are represented as A_n. In the substrate binding mode, E·A_n, the 3′-terminus of the RNA binds in the polyA subsite (as described in Figure 1B), and the ATP subsite is available to bind ATP such that subsequent adenylyl transfer can occur. In the product binding mode, E′·A_n, the 3′-terminal residue of polyA occupies the ATP subsite such that PP_i binding and subsequent pyrophosphorolysis can occur. Note that the internal step involves the conversion of central complexes (E·A_n·ATP ↔ E′·A_n·PP_i). This mechanism is identical in form to the general rapid equilibrium random mechanism (eq 1), but differs in the definitions of certain Michaelis constants. These differences reflect the fact that the formation of two enzyme·polyA binary complexes, E·A_n (forward direction) and E′·A_n (reverse direction), is possible. The observed A_n binding constant (for this mechanism), K_{ia}, is a composite of the two dissociation constants for these two enzyme species, K_1 and K_7. Furthermore, the K_m terms for both ATP (K_b) and PP_i (K_p) include a factor which reflects the proportion of the total population of the enzyme·A_n binary complex to which each reactant productively binds (*53*). This differs from the ordinary rapid equilibrium random case in which these

Table 2: Steady-State Kinetic Parameters of PAP

polyadenylation direction	pyrophosphorolysis direction
$K_a = K_4$	$K_a' = K_6$
$K_{ia} = 1/(1/K_1 + 1/K_7)$	$K_p = K_5(1 + K_7/K_1)$
$K_b = K_3(1 + K_1/K_7)$	$K_{ip} = K_8$
$K_{ib} = K_2$	

Michaelis constants are equal to the actual dissociation constants of these reactants from their ternary enzyme−substrate or −product complexes (*52*). Note that the large value of K_p (700 μM) relative to K_{ip} (30 μM) is consistent with either of two explanations (each representing an extreme case): either $K_7 \gg K_1$ (in which case, $K_5 \cong K_8$) or $K_5 \gg K_8$ (in which case, $K_1 \cong K_7$). The definitions of all the steady-state kinetic parameters in terms of the actual equilibrium dissociation constants depicted in Scheme 1 were derived by Chao et al. (*53*) and are provided in Table 2.

Several quantitative conclusions are derived from the data. Using the Haldane relationship for this mechanism (*54*) and the values reported in Table 1, the overall equilibrium constant, K_{eq}, can be calculated: $K_{eq} = (V_1K_p)/(V_2K_b) = 84$, corresponding to a ΔG of −2.7 kcal/mol (this is specific for 30 °C, pH 7, and 10 mM Mg^{2+}). From the published ΔG values for the hydrolysis of the α,β-phosphoanhydride of ATP [−11 kcal/mol (*65*)] and the condensation of a single stranded ribonucleic acid and nucleotide monophosphate [9 kcal/mol (*66*)], one estimates the free energy change for polyadenylate adenylation to be approximately −2 kcal/mol, which is in reasonable agreement with our experimentally derived value. This is very different from the template-dependent DNA and RNA polymerases for which there is realized a large, favorable change in free energy upon daughter strand synthesis (*67*) derived from both Watson−Crick base pairing and base stacking (*68*). The apparent internal equilibrium constant (K_{int}) for the ATP reaction with A_{18} can also be evaluated for this mechanism by $V_1/V_2 = 4$, corresponding to a ΔG of −0.8 kcal/mol. From these values, it is evident that the ternary complexes (E·A_n·ATP and E′·A_n·PP_i) are closer in free energy than the free substrates and products, and the difference between the free energy change that occurs in the overall process (K_{eq}) and in the central step (K_{int}) is 1.9 kcal/mol. We hypothesize that this free energy is conserved during the catalytic cycle by the formation of a higher-energy conformational state. This would constitute enzyme strain that is introduced after the chemical step, upon formation of the ternary enzyme−product complex (E′·A_n·PP_i). Furthermore, the initial velocity data from the pyrophosphorolysis reaction suggest that this strain is manifested primarily in the relatively large Michaelis constant for A_n in the reverse direction ($K_a' = 2$ mM). Thus, it follows that the consequence of the internal thermodynamics of the enzyme (which effectively increases the free energy of the E′·A_n·PP_i complex relative to that of the E·A_n·ATP complex) is to promote product A_n dissociation during the catalytic cycle and to exclude unproductive A_n (product mode) binding. Understanding the molecular basis of this phenomenon will require the structural characterization of both the enzyme−substrate and −product ternary complexes. Product A_n dissociation is of particular physiological importance because the enzyme is believed to operate under effectively saturating polyadenylate concentrations in vivo due to the function of RNA-binding proteins which are

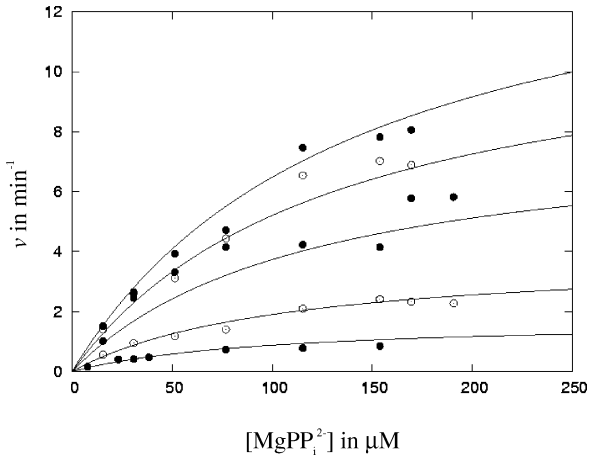

FIGURE 5: Initial velocity of pyrophosphorolysis by PAP. The initial velocity of pyrophosphorolysis at 10 mM Mg^{2+} as a function of $MgPP_i^{2-}$ concentration at various, fixed A_{18} concentrations is shown. The data sets (from bottom to top) correspond to 21.1, 47.8, 102.2, 153.4, and 204.5 μM A_{18}. The curves were generated using the experimentally derived parameters (reported in Table 1).

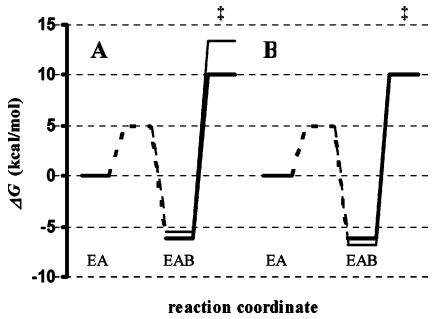

FIGURE 6: Free energy diagram for the PAP reaction with ATP and alternative substrates. A summary of the free energy changes realized for the reaction segment between nucleotide binding to the enzyme-A_n binary complex through formation of the transition state (E·A_n + NTP ↔ E·A_n·NTP ↔ [E·A_n·NTP]‡) is shown, where A is A_n, B is the nucleotide, and EA and EAB represent enzyme binary and ternary complexes, respectively. The E·A_n binary complex was taken as the reference state, and the relative energy levels for the EAB states and transition states were calculated in the usual manner using K_b and V_1, respectively (K_b is assumed to approximate a binding constant). The two sets of curves compare the reactions utilizing (A) ATP vs CTP and (B) ATP vs αS-ATP; in both cases, the bold lines depict data for the reaction of ATP. The dashed lines correspond to the barriers for nucleotide binding, for which no value is calculated.

associated with the CPF complex (*22*). It is apparent that the thermodynamics of the system favors the substrate mode over the product mode of binding of A_n. It should also be noted that binding of ATP and A_n (product mode) is mutually exclusive. Thus, under physiological conditions, the forward (polyadenylation) direction of the reaction would be very strongly favored.

The purpose of the experiments studying the reaction of CTP and the effects of α-thio substitution was to address the issue of nucleotide specificity. These results are summarized as free energy diagrams in Figure 6. The results demonstrate that the ground-state binding energies of either the correct (ATP) or incorrect (CTP) nucleotide substrate are very similar. By inspection of the free energy profile in Figure 6A, it is also evident that reduction of the free energy of the transition state (i.e., transition-state stabilization) of ATP, relative to that of CTP, almost entirely accounts for

nucleotide specificity in this case. This observation, however, does not satisfactorily explain the mechanism by which the enzyme specifically promotes catalysis upon the recognition of the adenine moiety of ATP, since the adenine moiety does not directly participate in chemistry. The qualitatively different sulfur elemental effects on V/K_m observed for ATP and CTP, however, provide significant insight into the mechanism of nucleotide specificity. The elemental effect of unity that was observed for ATP (Figure 6B) is indicative of a ground-state destabilization mechanism, the effect of which is to reduce the $\Delta G^{\ddagger}$ by increasing the free energy of the ground state without affecting the energy of the transition state (*63*). The biological purpose of ground-state destabilization is to utilize the intrinsic ground-state binding energy of a substrate to enhance the reaction velocity (*64*). The elemental effect on V/K_m for CTP of 3 indicates that this ground-state destabilization mechanism is not employed for the incorrect nucleotide. We therefore deduce that there must be a larger intrinsic binding energy for ATP that is not realized in the ground-state binding constant (the ground-state binding energies discussed here and depicted in Figure 6 are derived from the values of K_b). Presumably, this enhanced binding energy is derived from additional interactions between the adenine moiety of ATP and the enzyme. This proposal, derived simply from the transition-state theory of enzyme catalysis (*69*), states that the proper recognition of ATP by PAP in the Michaelis complex is characterized by the stabilization of both the ground state and the transition state. This concept has been described as "uniform binding" (*70*, *71*) or "distant binding" (*72*), and is predicted to involve portions of the substrate that are distant from the reactive part of the molecule. Because the effect of uniform binding is to increase V/K_m, this mechanism can account for nucleotide specificity. As mentioned above, crystallographic studies have identified specific active site residues that interact with or are in the proximity of the adenine of the nucleotide substrate (*33*−*35*). These residues include (yeast numbers) N189 and T304, and are depicted in Figure 1B. Martin et al. (*35*) reported that the mutation of bovine residue N202 (equivalent to yeast N189) to alanine had essentially no effect on the apparent K_m for ATP, but had a pronounced (10^2-fold reduction) effect on the apparent V_{max}. This result is consistent with the model proposed here, suggesting that this residue is particularly important in the recognition of the adenine of ATP (note the analogy between this result and that of the experiment involving the reaction of CTP, reported in Table 1). In summary, the combination of uniform binding of ATP (substrate specificity) and the utilization of ground-state destabilization of the E·A_n·ATP complex (rate acceleration) can comprehensively be considered as the induced fit mechanism of PAP and explains the thermodynamics of nucleotide specificity.

REFERENCES

1. Twu, J. S., and Bretthauer, R. K. (1971) Properties of a polyriboadenylate polymerase isolated from yeast ribosomes, *Biochemistry 10*, 1576−1582.
2. Hafe, L. A., and Keller, E. B. (1975) The polyadenylate polymerases from yeast, *J. Biol. Chem. 250*, 1838−1846.
3. Wahle, E. (1991) Purification and characterization of a mammalian polyadenylate polymerase involved in the 3′ end processing of messenger RNA precursors, *J. Biol. Chem. 266*, 3131−3139.
4. Lingner, J., Radtke, I., Wahle, E., and Keller, W. (1991) Purification and characterization of poly(A) polymerase from *Saccharomyces cerevisiae*, *J. Biol. Chem. 266*, 8741−8746.
5. Colgan, D. F., and Manley, J. L. (1997) Mechanism and regulation of mRNA polyadenylation, *Genes Dev. 11*, 2755−2766.
6. Zhao, J., Hyman, L., and Moore, C. (1999) Formation of mRNA 3′ ends in eukaryotes: Mechanism, regulation, and interrelationships with other steps in mRNA synthesis, *Microbiol. Mol. Biol. Rev. 63*, 405−445.
7. Chen, J., and Moore, C. (1992) Separation of factors required for cleavage and polyadenylation of yeast pre-mRNA, *Mol. Cell. Biol. 12*, 3470−3481.
8. Kessler, M. M., Zhao, J., and Moore, C. L. (1996) Purification of the *Saccharomyces cerevisiae* cleavage/polyadenylation factor I. Separation into two components that are required for both cleavage and polyadenylation of mRNA 3′ ends, *J. Biol. Chem. 271*, 27167−27175.
9. Minvielle-Sebastia, L., Preker, P. J., Wiederkehr, T., Strahm, Y., and Keller, W. (1997) The major yeast poly(A)-binding protein is associated with cleavage factor IA and functions in premessenger RNA 3′-end formation, *Proc. Natl. Acad. Sci. U.S.A. 94*, 7897−7902.
10. Zhao, J., Kessler, M. M., and Moore, C. L. (1997) Cleavage factor II of *Saccharomyces cerevisiae* contains homologues to subunits of the mammalian cleavage/polyadenylation specificity factor and exhibits sequence-specific, ATP-dependent interaction with precursor RNA, *J. Biol. Chem. 272*, 10831−10838.
11. Gross, S., and Moore, C. (2001) Five subunits are required for reconstitution of the cleavage and polyadenylation activities of *Saccharomyces cerevisiae* cleavage factor I, *Proc. Natl. Acad. Sci. U.S.A. 98*, 6080−6085.
12. Gilmartin, G. M., and Nevins, J. R. (1989) An ordered pathway of assembly of components required for polyadenylation site recognition and processing, *Genes Dev. 3*, 2180−2190.
13. Christofori, G., and Keller, W. (1988) 3′ cleavage and polyadenylation of mRNA precursors in vitro requires a poly(A) polymerase, a cleavage factor, and a snRNP, *Cell 54*, 875−889.
14. Takagaki, Y., Ryner, L. C., and Manley, J. L. (1988) Separation and characterization of a poly(A) polymerase and a cleavage/specificity factor required for pre-mRNA polyadenylation, *Cell 52*, 731−742.
15. Butler, J. S., and Platt, T. (1988) RNA processing generates the mature 3′ end of yeast CYC1 messenger RNA in vitro, *Science 242*, 1270−1274.
16. Christofori, G., and Keller, W. (1989) Poly(A) polymerase purified from HeLa cell nuclear extract is required for both cleavage and polyadenylation of pre-mRNA in vitro, *Mol. Cell. Biol. 9*, 193−203.
17. Terns, M. P., and Jacob, S. T. (1989) Role of poly(A) polymerase in the cleavage and polyadenylation of mRNA precursor, *Mol. Cell. Biol. 9*, 1435−1444.
18. Takagaki, Y., Ryner, L. C., and Manley, J. L. (1989) Four factors are required for 3′-end cleavage of pre-mRNAs, *Genes Dev. 3*, 1711−1724.
19. Bienroth, S., Wahle, E., Suter-Crazzolara, C., and Keller, W. (1991) Purification of the cleavage and polyadenylation factor involved in the 3′-processing of messenger RNA precursors, *J. Biol. Chem. 266*, 19768−19776.
20. Gilmartin, G. M., and Nevins, J. R. (1991) Molecular analyses of two poly(A) site-processing factors that determine the recognition and efficiency of cleavage of the pre-mRNA, *Mol. Cell. Biol. 11*, 2432−2438.
21. Wahle, E. (1995) Poly(A) tail length control is caused by termination of processive synthesis, *J. Biol. Chem. 270*, 2800−2808.
22. Bienroth, S., Keller, W., and Wahle, E. (1993) Assembly of a processive messenger RNA polyadenylation complex, *EMBO J. 12*, 585−594.
23. Edmonds, M. (1990) Polyadenylate polymerases, *Methods Enzymol. 181*, 161−170.
24. Preker, P. J., Ohnacker, M., Minvielle-Sebastia, L., and Keller, W. (1997) A multisubunit 3′ end processing factor from yeast containing poly(A) polymerase and homologues of the subunits of mammalian cleavage and polyadenylation specificity factor, *EMBO J. 16*, 4727−4737.

25. Zhao, J., Kessler, M., Helmling, S., O'Connor, J. P., and Moore, C. (1999) Pta1, a component of yeast CF II, is required for both cleavage and poly(A) addition of mRNA precursor, *Mol. Cell. Biol. 19*, 7733−7740.
26. Ohnacker, M., Barabino, S. M., Preker, P. J., and Keller, W. (2000) The WD-repeat protein pfs2p bridges two essential factors within the yeast pre-mRNA 3′-end-processing complex, *EMBO J. 19*, 37−47.
27. Gross, S., and Moore, C. L. (2001) Rna15 interaction with the A-rich yeast polyadenylation signal is an essential step in mRNA 3′-end formation, *Mol. Cell. Biol. 21*, 8045−8055.
28. Helmling, S., Zhelkovsky, A., and Moore, C. L. (2001) Fip1 regulates the activity of poly(A) polymerase through multiple interactions, *Mol. Cell. Biol. 21*, 2026−2037.
29. He, X., Khan, A. U., Cheng, H., Pappas, D. L., Jr., Hampsey, M., and Moore, C. L. (2003) Functional interactions between the transcription and mRNA 3′ end processing machineries mediated by Ssu72 and Sub1, *Genes Dev. 17*, 1030−1042.
30. Kerwitz, Y., Kuhn, U., Lilie, H., Knoth, A., Scheuermann, T., Friedrich, H., Schwarz, E., and Wahle, E. (2003) Stimulation of poly(A) polymerase through a direct interaction with the nuclear poly(A) binding protein allosterically regulated by RNA, *EMBO J. 22*, 3705−3714.
31. Kyburz, A., Sadowski, M., Dichtl, B., and Keller, W. (2003) The role of the yeast cleavage and polyadenylation factor subunit Ydh1p/Cft2p in pre-mRNA 3′-end formation, *Nucleic Acids Res. 31*, 3936−3945.
32. Nedea, E., He, X., Kim, M., Pootoolal, J., Zhong, G., Canadien, V., Hughes, T., Buratowski, S., Moore, C. L., and Greenblatt, J. (2003) Organization and function of APT, a subcomplex of the yeast cleavage and polyadenylation factor involved in the formation of mRNA and small nucleolar RNA 3′-ends, *J. Biol. Chem. 278*, 33000−33010.
33. Bard, J., Zhelkovsky, A. M., Helmling, S., Earnest, T. N., Moore, C. L., and Bohm, A. (2000) Structure of yeast poly(A) polymerase alone and in complex with 3′-dATP, *Science 289*, 1346−1349.
34. Martin, G., Keller, W., and Doublie, S. (2000) Crystal structure of mammalian poly(A) polymerase in complex with an analog of ATP, *EMBO J. 19*, 4193−4203.
35. Martin, G., Moglich, A., Keller, W., and Doublie, S. (2004) Biochemical and structural insights into substrate binding and catalytic mechanism of mammalian poly(A) polymerase, *J. Mol. Biol. 341*, 911−925.
36. Zhelkovsky, A. M., Kessler, M. M., and Moore, C. L. (1995) Structure−function relationships in the *Saccharomyces cerevisiae* poly(A) polymerase. Identification of a novel RNA binding site and a domain that interacts with specificity factor(s), *J. Biol. Chem. 270*, 26715−26720.
37. Martin, G., and Keller, W. (1996) Mutational analysis of mammalian poly(A) polymerase identifies a region for primer binding and catalytic domain, homologous to the family X polymerases, and to other nucleotidyltransferases, *EMBO J. 15*, 2593−2603.
38. Zhelkovsky, A., Helmling, S., and Moore, C. (1998) Processivity of the *Saccharomyces cerevisiae* poly(A) polymerase requires interactions at the carboxyl-terminal RNA binding domain, *Mol. Cell. Biol. 18*, 5942−5951.
39. Martin, G., Jeno, P., and Keller, W. (1999) Mapping of ATP binding regions in poly(A) polymerases by photoaffinity labeling and by mutational analysis identifies a domain conserved in many nucleotidyltransferases, *Protein Sci. 8*, 2380−2391.
40. Aravind, L., and Koonin, E. V. (1999) DNA polymerase β-like nucleotidyltransferase superfamily: Identification of three new families, classification and evolutionary history, *Nucleic Acids Res. 27*, 1609−1618.
41. Burgers, P. M., and Eckstein, F. (1979) A study of the mechanism of DNA polymerase I from *Escherichia coli* with diastereomeric phosphorothioate analogs of deoxyadenosine triphosphate, *J. Biol. Chem. 254*, 6889−6893.
42. Pelletier, H., Sawaya, M. R., Kumar, A., Wilson, S. H., and Kraut, J. (1994) Structures of ternary complexes of rat DNA polymerase β, a DNA template-primer, and ddCTP, *Science 264*, 1891−1903.
43. Sawaya, M. R., Pelletier, H., Kumar, A., Wilson, S. H., and Kraut, J. (1994) Crystal structure of rat DNA polymerase β: Evidence for a common polymerase mechanism, *Science 264*, 1930−1935.
44. Steitz, T. A., Smerdon, S. J., Jager, J., and Joyce, C. M. (1994) A unified polymerase mechanism for nonhomologous DNA and RNA polymerases, *Science 266*, 2022−2025.
45. Li, F., Xiong, Y., Wang, J., Cho, H. D., Tomita, K., Weiner, A. M., and Steitz, T. A. (2002) Crystal structures of the *Bacillus stearothermophilus* CCA-adding enzyme and its complexes with ATP or CTP, *Cell 111*, 815−824.
46. Sakon, J., Liao, H. H., Kanikula, A. M., Benning, M. M., Rayment, I., and Holden, H. M. (1993) Molecular structure of kanamycin nucleotidyltransferase determined to 3.0-Å resolution, *Biochemistry 32*, 11977−11984.
47. Pedersen, L. C., Benning, M. M., and Holden, H. M. (1995) Structural investigation of the antibiotic and ATP-binding sites in kanamycin nucleotidyltransferase, *Biochemistry 34*, 13305−13311.
48. Delarue, M., Boule, J. B., Lescar, J., Expert-Bezancon, N., Jourdan, N., Sukumar, N., Rougeon, F., and Papanicolaou, C. (2002) Crystal structures of a template-independent DNA polymerase: Murine terminal deoxynucleotidyltransferase, *EMBO J. 21*, 427−439.
49. Xiong, Y., Li, F., Wang, J., Weiner, A. M., and Steitz, T. A. (2003) Crystal structures of an archaeal class I CCA-adding enzyme and its nucleotide complexes, *Mol. Cell 12*, 1165−1172.
50. Ford, S. R., and Leach, F. R. (1998) Improvements in the application of firefly luciferase assays, *Methods Mol. Biol. 102*, 3−20.
51. Frey, C. M., Banyasz, J. L., and Stuehr, J. E. (1972) Interactions of divalent metal ions with inorganic and nucleoside phosphates. II. Kinetics of magnesium(II) with $HP_3O_{10}^{4-}$, ATP, CTP, $HP_2O_7^{3-}$, ADP, and CDP, *J. Am. Chem. Soc. 94*, 9198−9204.
52. Cleland, W. W. (1963) The kinetics of enzyme-catalyzed reactions with two or more substrates or products. I. Nomenclature and rate equations, *Biochim. Biophys. Acta 67*, 104−137.
53. Chao, J., Johnson, G. F., and Graves, D. J. (1969) Kinetic mechanism of maltodextrin phosphorylase, *Biochemistry 8*, 1459−1466.
54. Gold, A. M., Johnson, R. M., and Tseng, J. K. (1970) Kinetic mechanism of rabbit muscle glycogen phosphorylase a, *J. Biol. Chem. 245*, 2564−2572.
55. Gold, M. H., Farrand, R. J., Livoni, J. P., and Segel, I. H. (1974) *Neurospora crassa* glucogen phosphorylase: Interconversion and kinetic properties of the "active" form, *Arch. Biochem. Biophys. 161*, 515−527.
56. Sander, C., and Ts'o, P. O. (1971) Interaction of nucleic acids. 8. Binding of magnesium ions by nucleic acids, *J. Mol. Biol. 55*, 1−21.
57. Igarashi, K., Aoki, Y., and Hirose, S. (1977) Base specificity of polyamine binding to synthetic polynucleotides, *J. Biochem. 81*, 1091−1096.
58. Rudolph, F. B., and Fromm, H. J. (1971) Computer simulation studies with yeast hexokinase and additional evidence for the random bi bi mechanism, *J. Biol. Chem. 246*, 6611−6619.
59. Cleland, W. W., and Wratton, C. C. (1969) Studies on the Kinetic Mechanism of Liver Alcohol Dehydrogenase, in *The Mechanism of Action of Dehydrogenases* (Schwert, G. W., and Winer, A. D., Eds.) pp 103−124, The University Press of Kentucky, Lexington, KY.
60. Benkovic, S. J., and Schray, K. J. (1973) The Chemistry of Phosphoryl Transfer, in *The Enzymes* (Boyer, P. D., Ed.) Vol. VIII, pp 201−236, Academic Press, New York.
61. Benkovic, S. J., and Schray, K. J. (1978) Phosphoryl Transfer, in *Transition States of Biochemical Processes* (Gandoor, R. D., Ed.) pp 493−527, Plenum, New York.
62. Herschlag, D., Piccirilli, J. A., and Cech, T. R. (1991) Ribozyme-catalyzed and nonenzymatic reactions of phosphate diesters: Rate effects upon substitution of sulfur for a nonbridging phosphoryl oxygen atom, *Biochemistry 30*, 4844−4854.
63. Fersht, A. R. (1974) Catalysis, binding and enzyme−substrate complementarity, *Proc. R. Soc. London, Ser. B 187*, 397−407.
64. Herschlag, D. (1988) The role of induced fit and conformational changes of enzyme in specificity and catalysis, *Bioorg. Chem. 16*, 62−96.
65. Frey, P. A., and Arabshahi, A. (1995) Standard free energy change for the hydrolysis of the α,β-phosphoanhydride bridge in ATP, *Biochemistry 34*, 11307−11310.
66. Peller, L. (1976) On the free-energy changes in the synthesis and degradation of nucleic acids, *Biochemistry 15*, 141−146.
67. Kuchta, R. D., Mizrahi, V., Benkovic, P. A., Johnson, K. A., and Benkovic, S. J. (1987) Kinetic mechanism of DNA polymerase I (Klenow), *Biochemistry 26*, 8410−8417.

68. Bloomfield, V. A., Crothers, D. M., and Tinoco, I., Jr. (1974) *Physical Chemistry of Nucleic Acids*, Harper Row, New York.
69. Pauling, L. (1946) Molecular architecture and biological reactions, *Chem. Eng. News 24*, 1375−1377.
70. Albery, W. J., and Knowles, J. R. (1976) Evolution of enzyme function and the development of catalytic efficiency, *Biochemistry 15*, 5631−5640.
71. Burbaum, J. J., Raines, R. T., Albery, W. J., and Knowles, J. R. (1989) Evolutionary optimization of the catalytic effectiveness of an enzyme, *Biochemistry 28*, 9293−9305.
72. Warshel, A. (1998) Electrostatic origin of the catalytic power of enzymes and the role of preorganized active sites, *J. Biol. Chem. 273*, 27035−27038.

BI050089R